PAPER

First principles high throughput screening of oxynitrides for water-splitting photocatalysts

Yabi Wu,[a] Predrag Lazic,[a] Geoffroy Hautier,†[a] Kristin Persson[b] and Gerbrand Ceder*[a]

In this paper, we present a first principles high throughput screening system to search for new water-splitting photocatalysts. We use the approach to screen through nitrides and oxynitrides. Most of the known photocatalytic materials in the screened chemical space are reproduced. In addition, sixteen new materials are suggested by the screening approach as promising photocatalysts, including three binary nitrides, two ternary oxynitrides and eleven quaternary oxynitrides.

Broader context

Water-splitting photocatalysis directly converts the solar energy to chemical energy and is involved in many applications in energy and environmental science. Finding novel photocatalytic materials that are stable, efficient, and capable of being visible light driven is the primary objective in this field. In this paper, we present a recently finished first principles high throughput screening to identify nitride and oxynitride candidate compounds as novel water-splitting photocatalysts. 68 nitrides, 1503 ternary oxynitrides and 1377 quaternary oxynitrides are screened based on their properties of phase stability, band gap and band edge positions. Most of the known photocatalytic materials in the screened chemical space are reproduced. In addition, sixteen new materials, including three binary nitrides, two ternary oxynitrides and eleven quaternary oxynitrides, are identified as promising water-splitting photocatalysts. They are predicted to be synthesizable, suitable for visible light (or UV light) absorption, and energetically favorable to catalyze the water-splitting reaction. Three of these sixteen candidates, $Ti_3O_3N_2$, $La_2TiO_2N_2$ and Li_5MoO_4N, have potentials to exhibit better photocatalytic performance than the best oxynitride photocatalysts known today.

I Introduction

Since the discovery of the first photocatalytic water splitting system based on TiO_2 and Pt in 1972 by Fujishima and Honda,[1,2] the photocatalysis of water splitting has become an active research area and a promising way to capture and store energy from the Sun. More than 130 inorganic materials have been demonstrated to exhibit such photocatalytic performance.[3] However, the overall efficiency of current water-splitting photocatalytic devices is still well below a commercially viable level.[3] The primary objective in the field is to find new materials with higher efficiency.

High throughput computational screening whereby one computationally assesses key properties of a large number of compounds for a given application has shown its merit in many fields, such as the design of new battery materials,[4–7] thermo-electric materials,[8,9] piezoelectric materials,[10] and organic photovoltaic materials.[11–13] The development of *ab initio* property prediction methods and their automation make it possible to examine thousands of material candidates for a few desired properties.[14,15]

In this paper, we screen compounds using high throughput computational methods by focusing on three significant properties of water-splitting photocatalysts: (1) the crystal structure and its thermodynamic phase stability (*versus* competing solids and gases); (2) the band gap; (3) the conduction band (CB) and valence band (VB) edge positions relative to the H_2/H_2O and O_2/H_2O levels in water. For each property, a first principles computational method has been developed which has a low enough computational cost but an adequate accuracy so that it can be used in a high throughput search. By integrating them, we thus design a 3-tier high throughput screening system as follows: (a) a phase stability screening to eliminate candidate compounds which are not stable enough to be synthesizable; (b) a band gap screening to eliminate all candidates with a too large or too small band gap; (c) a screening of band edge position in aqueous environment to eliminate candidates whose CB or VB position is not suitable for water splitting. The details of the screening system are introduced in Section II.

We choose oxynitrides as the major chemical space to implement the screening system in this work. So far, most of the existing photocatalysts are oxides.[3] However, the band gaps of oxides are usually too large to absorb visible light.[3,16] This is mainly due to a too low VB energy which is derived from the 2p orbitals of the oxygen atoms.[16] To solve this problem, non-oxides such as nitrides and sulfides have been proposed, since

[a] *Department of Materials Science and Engineering Massachusetts Institute of Technology, Cambridge, Massachusetts 02139, USA*

[b] *Lawrence Berkeley National Laboratory, 1 Cyclotron Rd, Berkeley, California 94720, USA*

† Current address: Institut de la matière condensée et des nanosciences (IMCN), European Theoretical Spectroscopy Facility (ETSF), Université Catholique de Louvain, Chemin des étoiles 8, bte L7.03.01, 1348 Louvain-la-Neuve, Belgium

This journal is © The Royal Society of Chemistry 2013

Energy Environ. Sci., 2013, **6**, 157–168 | **157**

their VB position is usually higher in energy. Unfortunately, nitrides usually suffer from poor aqueous stability,[17] and cannot maintain photocatalytic activity in water over a long period of time. As a result, oxynitrides have been lately proposed[16] as a balance between band gap reduction and aqueous stability.

In this paper, we screened 2948 different candidate compounds including 68 binary nitrides, 1503 ternary oxynitrides and 1377 quaternary oxynitrides. Our algorithm picked out most of the known water-splitting photocatalysts and also found 16 new promising candidates. Some new candidates are existing materials from the Inorganic Crystal Structure Database (ICSD)[18] but have not been reported as photocatalysts yet. And some candidates are unknown compounds which are predicted by our compound prediction tool.[19] The detailed results are shown in Section III.

Very recently, Castelli *et al.* computationally screened perovskite metal oxides and identified some new candidates for photocatalysts.[20] The major differences between theirs and our screening approach are the following: (a) Castelli *et al.* predicted the CB and VB positions by empirically estimating the middle of the gap using electronegativity of the atoms while we compute them directly from first principles in an aqueous environment; (b) they mainly focused on perovskite metal oxides while we mainly focus on oxynitrides, and we consider a wider range of structures.

II Method

Fig. 1 illustrates the high throughput screening approach presented in this paper. All computations are based on density functional theory (DFT)[21,22] and are performed with projector augmented wave (PAW)[23] potentials using the plane-wave code Vienna *Ab initio* Simulation Package (VASP).[24,25] For computations in steps 1 and 2 in Fig. 1, we use the Perdew–Burke–Ernzerhof (PBE)[26] GGA+U exchange-correlation functional unless specified otherwise, with all parameters as in *Jain et al.*[14] For computations in step 3, we use PBE GGA with all parameters as described in ref. 27.

0 Generation of the candidates

In this step, we generate the candidate compounds for screening. As most known oxide photocatalysts contain d^{10} or

d^0 cations,[3,16] we target primarily oxynitrides and only consider compounds that contain d^{10} cations (Ga^{3+}, In^{3+}, Ge^{4+}, Sn^{4+}, Sb^{5+}, and Bi^{5+}) or d^0 cations (Ti^{4+}, Zr^{4+}, Hf^{4+}, V^{5+}, Nb^{5+}, Ta^{5+}, Cr^{6+}, Mo^{6+}, W^{6+}, Sc^{3+}, and Y^{3+}).

One of the most complete databases of experimentally observed compounds is the ICSD.[18] However, there are very few oxynitrides available in the ICSD. For example, there are only 25 ternary oxynitrides and 118 quaternary oxynitrides which contain d^{10} or d^0 cations in the ICSD. Therefore, we use compound and structure prediction tools[19] to identify possible novel compounds. Since the oxynitrides space has not been as exhaustively searched with experiments as other chemistries (*e.g.* oxides), it is likely that there are a large number of novel compounds to be found. We used a previously developed approach based on ionic substitutions to propose new likely ternary and quaternary oxynitrides.[19] This approach uses information about the substitution probability of ions – obtained by data-mining all known crystalline compounds – to come up with suggestions for the design of novel compounds.

To generate novel ternary oxynitrides (M–O–N, with M being a d^0 or d^{10} cation), we used the set of all known binary ionic compounds as a starting point. Using the substitution algorithm from ref. 19, we evaluated the likelihood that substituting the cation in each compound by M and the anion in the compound by a mixture of O and N would lead to a new stable compound. For instance, the algorithm suggested that the known Ta_3N_5 could have its cation Ta^{5+} substituted by Zr^{4+} and its anion N^{3-} by a mixture of O^{2-} and N^{3-}.

To generate new quaternary compounds (M1–M2–O–N with M1 or M2 being a d^0 or d^{10} cation), we only considered a list of known ternary oxide photocatalysts in ref. 3 as the structural framework on which to perform the substitutions. For instance, $SrTiO_3$ could lead to a new candidate from substituting Sr^{2+} by La^{3+}, Ti^{4+} by Ta^{5+}, and O^{2-} by a mixture of N^{3-} and O^{2-} according to the probabilistic model in ref. 19.

The amount of O and N to be substituted in each compound was determined by balancing the charge of the cations. There is however still a remaining degree of freedom in the exact ordering of O^{2-} and N^{3-} on the anion sites. We enumerated the different O^{2-}–N^{3-} orderings by using an algorithm similar to the one developed by Hart and Forcade[28] and selected the ones leading to the smaller cells and the larger number of N–N bonds, as the ordering of oxynitride anions has been recently shown to be driven by this factor.[29] For each candidate compound, we computed with DFT all selected orderings and only considered the one with lowest energy. It is worth noting that each possible compound also had to pass the stability screen in its relevant composition space (step 1 in Fig. 1) in order to be considered further.

Besides the oxynitrides, we included all binary nitrides M–N with M being a transition metal or semi-metal cation from the ICSD into the screening as well. Thus, in sum, we prepared 3 batches of candidate compounds, binary nitrides (M–N), ternary oxynitrides (M–O–N) and quaternary oxynitrides (M1–M2–O–N).
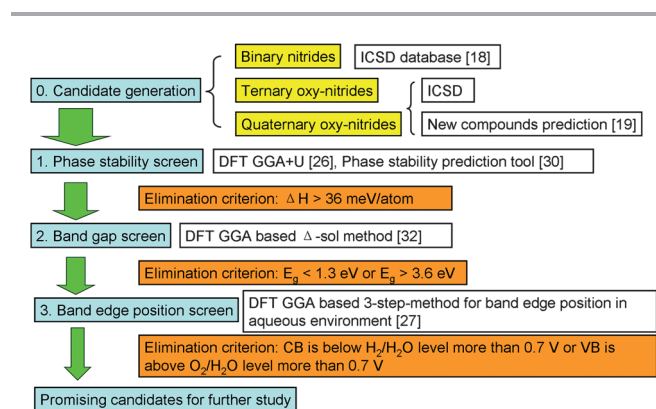

Fig. 1 High throughput screening approach for water-splitting photocatalysts.

1   Phase stability screening

Phase stability is an essential component of high-throughput materials discovery as new proposed candidates need to be stable enough to be synthesizable. To assess if a compound is stable at zero K, we compared its energy *versus* the energy of other phases or their linear combinations. This can be technically achieved through the convex hull construction.[30] Not only does the convex hull construction indicate if a compound is stable *versus* competing phases but this construction can also be used to assess how unstable a compound is. Therefore, we define the instability energy ΔH, in meV per atom, as the negative of the decomposition reaction energy to the stable phases. Stable compounds have an instability energy ΔH equal to zero and the larger the instability energy ΔH, the less stable the material is.

We performed this stability analysis for all compounds considered in this work. The possible competing phases were mainly obtained from the ICSD.[18] More details on the parameters used for the computations can be found in *Jain et al.*[14] In addition, we used a recently developed scheme to mix GGA and GGA+U computations[31] as computations of oxides and oxynitrides are usually performed with GGA+U while all nitrides have been computed with GGA.

In this screening, we eliminated all compounds with an instability energy ΔH larger than 36 meV per atom. We obtained this threshold energy by doing a brief analysis of the instability energy of compounds in the ICSD. We find that more than 80% of the ICSD compounds have an "instability energy ΔH" less than 36 meV per atom. Since the "ICSD compounds" have, in principle, all been synthesized, we consider this threshold to be reasonable to find compounds that can be made.

2   Band gap screening

In this step, we compute the band gap of the remaining candidates and eliminate those with unsuitable band gaps. Since the band gap computed from Kohn–Sham levels is usually lower than the experimental band gap by 30–100%,[32] this approach cannot be used for band gap screening. Alternatively, we use the Δ-sol method[32] to determine the gaps. The Δ-sol method, motivated by the dielectric screening properties of the homogeneous electron gas, determines the fundamental gap from DFT total energies of systems with an electron or a hole added within the screening radius of the material. Unreliable Kohn–Sham levels are not involved in the determination of the gap, and gross underestimation of band gaps is avoided. When tested across a large number of compounds with diverse chemistries, the Δ-sol method gave a mean absolute error of 0.2 eV for the gap.[32] In addition, the method requires three DFT total energy computations so it is acceptable in terms of computational cost. More detailed information is available in ref. 32.

In this screening step, we eliminate all candidates with band gaps lower than 1.3 eV or higher than 3.6 eV. The theoretical lower limit of the band gap for a water-splitting photocatalyst is 1.23 eV,[3] but an over-potential of 0.25 eV or more is usually required.[33,34] Therefore, the lowest possible band gap in practice

is around 1.5 eV. We further take the mean error of the Δ-sol method, around 0.2 eV, into account and finally set the lower threshold to 1.3 eV. The upper threshold is more flexible. For visible light absorption, 2.7 eV could be a good upper limit. However, we extend the upper limit to 3.6 eV to also capture any interesting oxynitride materials that absorb outside the visible light region.

3   Screening of band edge positions in aqueous environment

In this step, we compute the CB and VB band edge positions in aqueous environment and compare them with the H_2/H_2O and O_2/H_2O levels in water. We used an earlier developed 3-step method which is reported in ref. 27. In this method, the relevant energy levels (*e.g.* the CB of the semiconductor and the H_2/H_2O level in water) at the interface are considered as the corresponding bulk energy levels subjected to the interfacial band bending effect. Ref. 27 demonstrates that, for calculating the relative position between the CB and H_2/H_2O level at the interface, it is sufficient to separately compute the following three properties: the semiconductor's CB position relative to its Hartree potential; the H_2/H_2O level relative to water's Hartree potential; and the Hartree potential difference between the semiconductor and water in an aqueous environment. When tested on six typical photocatalysts, the method gave a mean absolute error of 0.19 eV for the band edge positions. More detailed information is available in ref. 27. Once we obtain the CB position relative to the H_2/H_2O level in water, it is straightforward to obtain the VB position relative to the O_2/H_2O level since the band gap has been computed in the previous step.

The photocatalytic water-splitting process is energetically favorable only if the CB is higher than the H_2/H_2O level and the VB is lower than the O_2/H_2O level. (Here and throughout this paper, "higher" always refers to more negative in the Normal Hydrogen Electrode reference while "lower" always refers to more positive in the NHE reference.) If this is not the case, then an external bias voltage is required to shift the bands to the right positions. However, applying an external bias voltage increases the complexity of the device and more importantly requires energy input to the device thus reducing the efficiency. As a result, too large a bias voltage should be avoided. We set the threshold of the allowed bias voltage as 0.7 V and eliminate all candidates whose CB is 0.7 eV lower than the H_2/H_2O level or whose VB is 0.7 eV higher than the O_2/H_2O level in water as shown in Fig. 2.
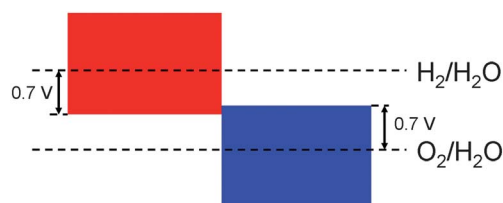

Fig. 2 Allowed CB and VB positions. The red shaded area represents the allowed CB positions while the blue shaded area represents the allowed VB positions.

III Results

1 Binary nitrides

We screened 68 different binary nitrides M–N where M consists of all transition metal elements and semi-metal elements. Since all the candidate compounds are obtained from the ICSD, we assume them to be synthesizable, so we do not present the results of their phase stability here. We find that 23 binary nitrides have a gap between 1.3 eV and 3.6 eV. These gaps and some experimental gap data (if available) are shown in Fig. 3. There is generally good agreement between computational band gaps and experimental band gaps.

For the 23 compounds with a suitable band gap, the band edge positions are calculated. All candidates not satisfying the band position criteria indicated in Fig. 2 are eliminated. The remaining candidates and their band levels are shown in Table 1.

The first three nitrides in Table 1, GaN, Ge_3N_4 and Ta_3N_5, are known as water-splitting photocatalysts.[17,44,45] Only for Ta_3N_5 the band edge positions have been experimentally measured,[16] and these values are included in Table 1 for comparison. Cu_3N, AgN_3, and Zr_3N_4 are known compounds but have not been reported as photocatalysts yet. We plot their band positions relative to the water redox levels in Fig. 4.
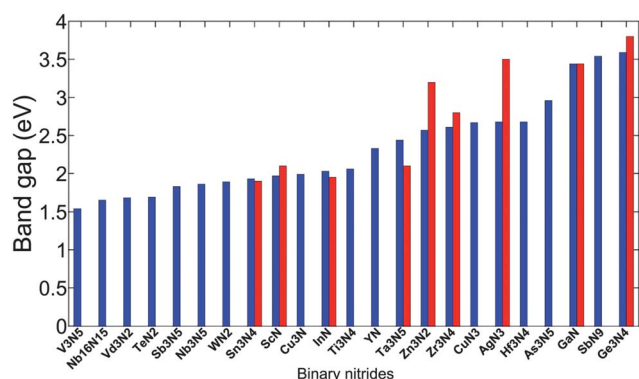
Fig. 3 Binary metal nitrides from the ISCD with a calculated band gap between 1.5 eV and 3.6 eV. The blue bars are computational band gaps while the red bars are experimental band gaps (if available). The experimental band gaps are collected from ref. 16 and 35–43.

Table 1 Identified binary nitride candidates[a]

Material	Band gap (eV)	CB vs. H_2/H_2O (eV)	VB vs. O_2/H_2O (eV)
GaN	3.49	−0.26	−2.63
Ge_3N_4	3.59	−0.31	−2.67
Ta_3N_5	2.37	0.66 (0.40 in exp)	−0.49 (−0.37 in exp)
Cu_3N	1.99	−0.31	−1.06
AgN_3	2.68	0.48	−0.97
Zr_3N_4	2.61	−0.58	−1.96

[a] In the column of "CB vs. H_2/H_2O" and "VB vs. O_2/H_2O", the number indicates how much the band edge is higher (more negative in the NHE reference) than the corresponding water level. Therefore, a positive number in the "CB vs. H_2/H_2O" column and a negative number in the "VB vs. O_2/H_2O" column is the optimum case as that indicates that the CB and VB are bracketing the water redox levels and no bias voltage is needed.
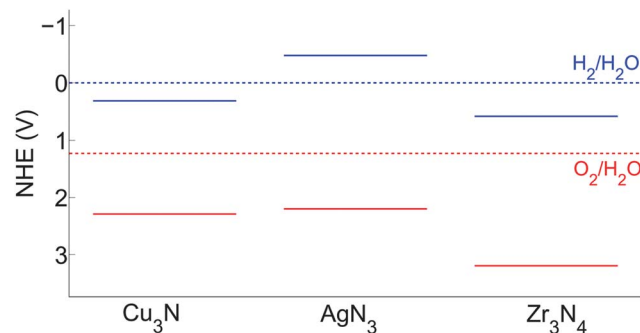

Fig. 4 Band edge positions of Cu_3N, AgN_3, and Zr_3N_4 in the normal hydrogen electrode (NHE) reference. The solid blue lines indicate the CB levels and the solid red lines indicate the VB levels.

Fig. 4 suggests that AgN_3 has its CB and VB bracketing the water redox levels, and thus may achieve water-splitting without an external bias voltage. However, its band gap, predicted to be 2.68 eV and experimentally measured as 3.5 eV, is suitable to absorb only UV light. Cu_3N has a VB lower than the O_2/H_2O level in water but its CB is 0.31 V lower than the H_2/H_2O level in water too. This indicates that H_2 evolution cannot be photo-catalyzed without applying an external bias voltage of at least 0.3 V. However, the band gap of Cu_3N, predicted to be 1.99 eV, is relatively small. This may provide enough optimization room to increase the CB while still retaining a reasonable gap. Similar to Cu_3N, Zr_3N_4 also has a too low CB and may need a bias voltage to photo-catalyze H_2 evolution. However, unlike Cu_3N, the band gap of Zr_3N_4, predicted to be 2.61 eV, is already relatively large and provides little optimization room to increase the CB. As a result, Zr_3N_4 is likely to be less efficient as a visible light driven photocatalyst.

Our screening of the binary nitrides reproduced three known binary photocatalysts, Ta_3N_5, GaN, and Ge_3N_4. In addition, we identified three known compounds as new candidates: Cu_3N, AgN_3, and Zr_3N_4. Cu_3N has the potential to be an efficient visible light driven photocatalyst, while AgN_3 and Zr_3N_4 are more likely to work under UV illumination.

2 Ternary oxynitrides

In this section, we screened 1503 different ternary oxynitrides, M–O–N, where M is one of the d^0 or d^{10} cations mentioned in Section II. The calculated phase stability of these compounds is shown in Fig. 5. As most of these compounds are computationally designed, it is not surprising that many of them are not stable as indicated by their large ΔH for decomposition in Fig. 5(a).

Fig. 5 indicates that all ternary oxynitrides consisting of V^{5+}, Cr^{6+}, Mo^{6+}, or Sb^{5+} are very unstable. This may be explained by the limited oxidation power of nitrogen gas. Support for this interpretation is the fact that there are no stable binary nitrides for V^{5+}, Cr^{6+}, Mo^{6+}, and Sb^{5+} in the ICSD. Moreover, we will show in Section IV that the required oxidizing power for these four cations is indeed the highest among all cations listed in Fig. 5. Fig. 5 also suggests that the majority of the stable and
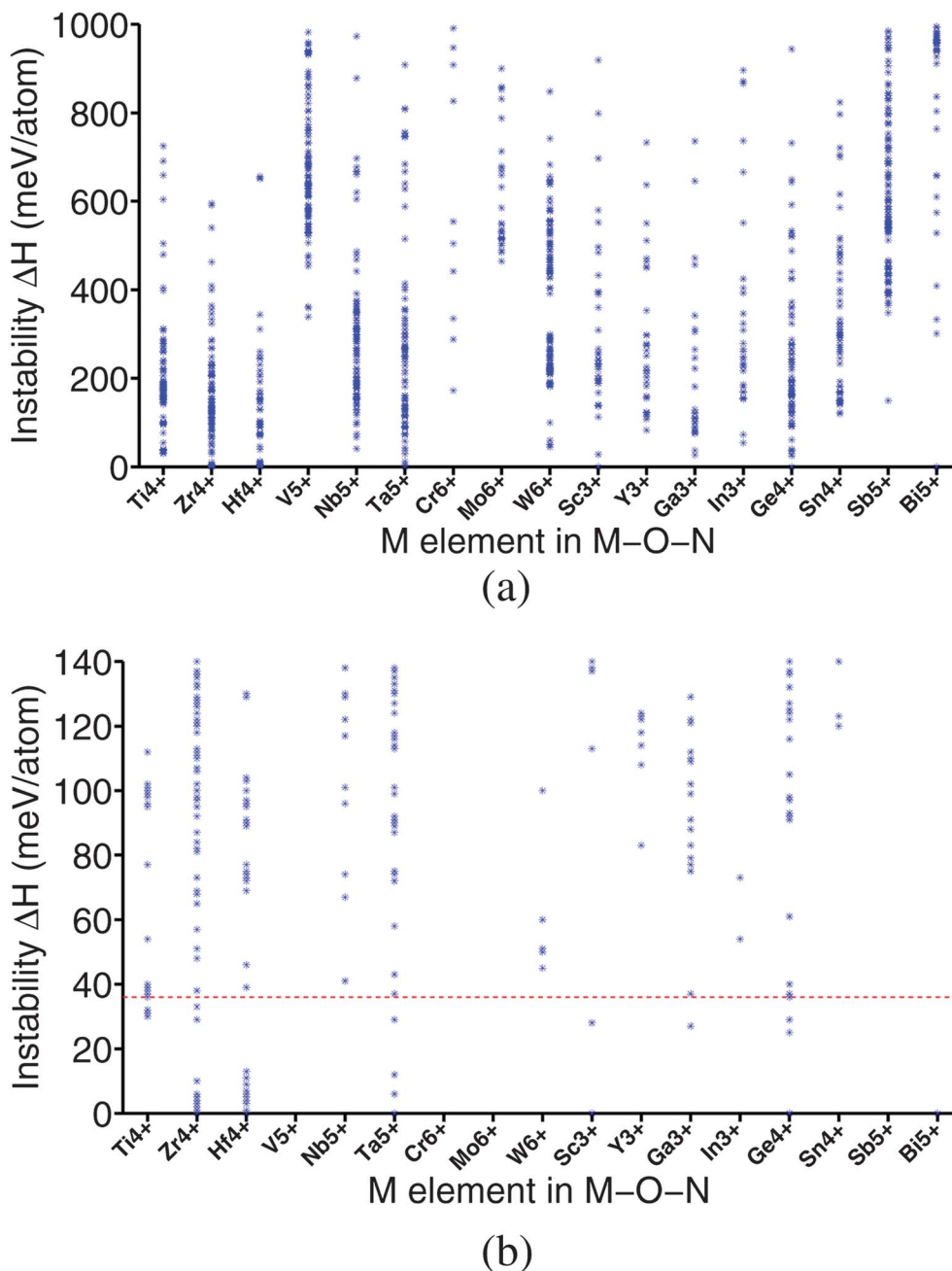
Fig. 5 Phase stability of ternary oxynitrides. Each point represents a different compound. The instability energy ΔH is defined in Section II. Larger ΔH indicates a larger instability. (a) All candidate compounds whose ΔH is less than 1000 meV per atom. (b) An enlarged version of (a) focusing on the stable and quasi-stable candidates region. The red dashed line in (b) represents the elimination criterion of this step, 36 meV per atom. All candidates above the red line were eliminated.

Table 2 Identified ternary oxynitride candidates[a]

Material	Reported/new	ΔH (meV per atom)	Band gap (eV)	CB vs. H_2/H_2O (eV)	VB vs. O_2/H_2O (eV)
TaON	Reported	0	2.83	0.64 (0.34 in exp)	−0.97 (−0.93 in exp)
Zr_2ON_2	Reported	0	2.57	−0.34	−1.67
$Ti_3O_3N_2$	New	31	2.37	0.22	−0.92
$Zr_3O_3N_2$	New	1	3.40	1.54	−0.63

[a] The numbers in the column of "CB vs. H_2/H_2O" and "VB vs. O_2/H_2O" have the same meaning as in Table 1.

quasi-stable ternary oxynitrides are obtained with Ti^{4+}, Zr^{4+}, Hf^{4+}, Ta^{5+}, Ga^{3+}, and Ge^{4+} which are much easier to oxidize.

After further screening of band gap and band edge positions, four ternary oxynitrides, TaON, Zr_2ON_2, $Zr_3O_3N_2$, and $Ti_3O_3N_2$, are identified as photocatalysts as shown in Table 2. Among the four ternary oxynitrides, TaON is a well known water-splitting photocatalyst.[16] Its band edge positions have been experimentally measured[16] and are given in Table 2 for comparison. Zr_2ON_2, while not present in the ICSD, has been reported as a promising material for photo-electrochemical water-splitting.[46] And the reported bixbyite structure for this compound is the same as our prediction, showing some validity of our structure prediction approach.

The remaining two materials, $Ti_3O_3N_2$ and $Zr_3O_3N_2$, have not been reported yet and are predicted by this work. Both compounds are generated from the crystal structure of Ta_3N_5. Their crystal structures are compared in Fig. 6. The instability energy ΔH is 31 meV per atom for $Ti_3O_3N_2$ and 1 meV per atom for $Zr_3O_3N_2$. This suggests that both materials are likely to be synthesizable. In fact, $Ti_3O_3N_2$ is declared to have been synthesized from a website.[47]

The band edge position shown in Fig. 7 suggests that $Ti_3O_3N_2$ is particularly interesting as its CB and VB bracket the water redox levels and its band gap, predicted to be 2.37 eV, is small enough for visible light absorption. Comparing the band properties of $Ti_3O_3N_2$ with TaON, the best oxynitride photocatalyst reported so far,[16] we find that both of them have their CB and VB bracketing the water redox levels, but the band gap of $Ti_3O_3N_2$ is expected to be smaller than the band gap of TaON (2.83 eV in our computation and 2.4 eV in experiment). Therefore, $Ti_3O_3N_2$ has a potential to exhibit better photocatalytic performance than TaON. $Zr_3O_3N_2$ also has its CB and VB bracketing the water redox levels, but its predicted band gap is large (3.40 eV). However, Fig. 7 suggests that the large band gap of $Zr_3O_3N_2$ is mainly due to its too high CB level. Shifting the CB downwards is a relatively easy band engineering problem which can be achieved with cation doping. If its CB can be shifted to be
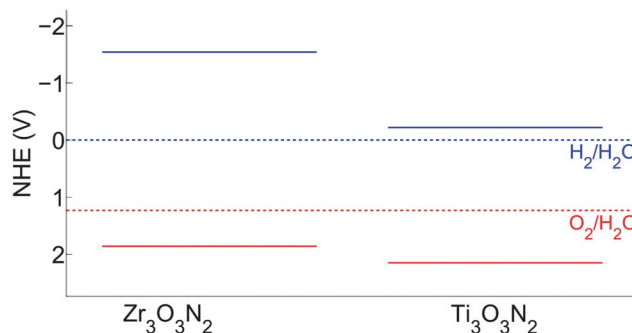

Fig. 7 Band edge position of $Ti_3O_3N_2$ and $Zr_3O_3N_2$ in the normal hydrogen electrode (NHE) reference. The solid blue lines indicate the CB levels and the solid red lines indicate the VB levels.

slightly higher than the H_2/H_2O level while retaining its VB position, the band gap will be reduced to 2.0 eV, making it a promising candidate for visible light driven photocatalysts.

In this section, we identified four materials, TaON, Zr_2ON_2, $Ti_3O_3N_2$, and $Zr_3O_3N_2$, as promising candidates for photocatalysts. TaON and Zr_2ON_2 are known photocatalysts and reproducing them from our screening system shows the validity of the approach. More importantly, we identified two new materials, $Ti_3O_3N_2$ and $Zr_3O_3N_2$. $Ti_3O_3N_2$ shows a very promising band gap and band edge positions, and has a potential to be a better visible-light driven photocatalyst than TaON. $Zr_3O_3N_2$ is predicted to be a good photocatalyst under UV illumination, and may also be visible light driven with some CB engineering. In addition, both $Zr_3O_3N_2$ and $Ti_3O_3N_2$ have the Ta_3N_5 structure, and thus solid solutions of these three materials are likely to be synthesizable, creating a large chemical space in which these materials can be optimized.

3 Quaternary oxynitrides

In this section, we screened 1377 quaternary oxynitrides, M1–M2–O–N, where M1 or M2 is a d^0 or d^{10} metal cation as described in Section II. Fig. 8 shows the combination of M1–M2 elements for which we find compounds with ΔH less than 0.2 eV per atom. We mentioned in Fig. 5 that some d^0 or d^{10} cations such as V^{5+}, Cr^{6+}, Mo^{6+}, and Sb^{5+} do not have stable corresponding ternary oxynitrides. In Fig. 8, we found that Cr^{6+}, Mo^{6+}, and Sb^{5+} do have some stable corresponding quaternary oxynitrides. This suggests that the required oxidizing power for these cations may decrease by adding a second metal cation into the system. It may also be noted that, for some d^0 or d^{10} cations which have stable corresponding ternary oxynitrides in Fig. 5, such as Zr^{4+} and Ga^{3+}, we have not found any corresponding quaternary oxynitrides in Fig. 8. This is because that, as we mentioned in Section II.0, our sampling in quaternary oxynitrides is not exhaustive but only based on a limited prototype of ternary oxides listed in ref. 3. It is possible that stable Zr^{4+} and Ga^{3+} quaternary oxynitrides exist but they cannot be derived from the prototypes we considered in this work. Another consequence of the limited sampling in quaternary oxynitrides is that some known quaternary oxynitride
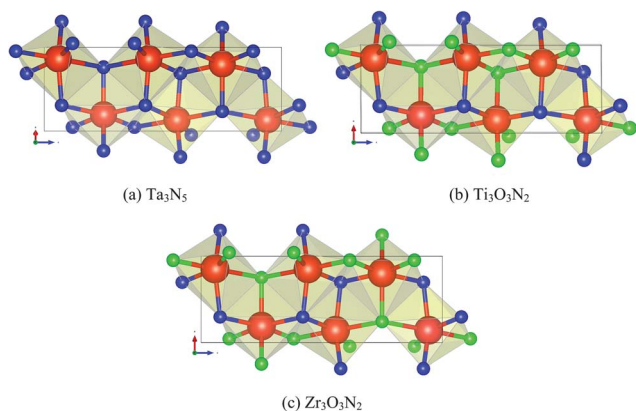

Fig. 6 Crystal structures of (a) Ta_3N_5, (b) $Ti_3O_3N_2$, and (c) $Zr_3O_3N_2$. Blue atoms are N, green atoms are O and red atoms are (a) Ta, (b) Ti, and (c) Zr. Structures (b) and (c) are generated by substituting all Ta atoms in (a) with Ti atoms and Zr atoms respectively and substituting 3/5 of the N atoms in (a) with O atoms. However, note that the positions of the O atoms in (b) and (c) are not identical.
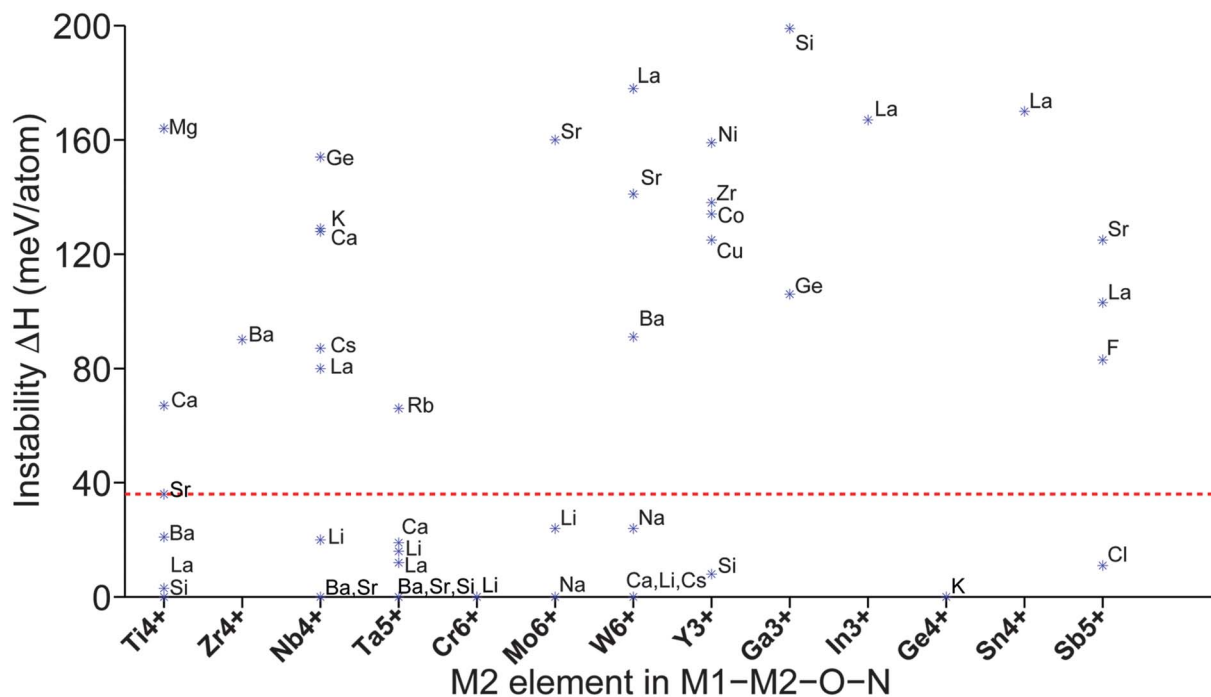
162 | *Energy Environ. Sci.*, 2013, **6**, 157–168

This journal is © The Royal Society of Chemistry 2013

Fig. 8 Phase stability of quaternary oxynitrides. Each point represents the lowest energy compound containing the two specified cations (*i.e.* a d^0 or d^{10} cation with another metal cation). We only show those pairs of cations which have at least one compound with ΔH less than 0.2 eV per atom. All candidates above the red dashed line (36 meV per atom) were eliminated.

photocatalysts ($SrNbO_2N$[48] for instance) were not reproduced by our screening since they could not be derived from the prototypes we considered.

After screening for band gap and band edge positions, seventeen compounds are identified as promising candidates for photocatalysts as shown in Table 3. Six of these compounds, $CaTaO_2N$,[49] $SrTaO_2N$,[49] $BaTaO_2N$,[49] $LaTaO_2N$,[50] $LaTiO_2N$,[51] and $BaNbO_2N$,[52] have been reported as water-splitting

photocatalysts. Experimentally measured band gaps for $CaTaO_2N$, $SrTaO_2N$, and $BaTaO_2N$ are reported as 2.4 eV, 2.1 eV, and 1.8 eV respectively and our calculated band gaps for these three compounds, 2.53 eV, 2.26 eV and 1.90 eV respectively, agree well with them. Moreover, the calculated band edge positions of these three compounds suggest that their VB is actually higher than the O_2/H_2O level. Therefore, they are unsuitable for photocatalyzing the O_2 evolution reaction without an external bias

Table 3 Identified quaternary oxynitride candidates[a]

Material	Reported/new	ΔH (meV per atom)	Band gap (eV)	CB *vs.* H_2/H_2O (eV)	VB *vs.* O_2/H_2O (eV)
$CaTaO_2N$	Reported	19	2.53	1.50	0.20
$SrTaO_2N$	Reported	0	2.26	1.34	0.31
$BaTaO_2N$	Reported	0	1.90	0.97	0.30
$LaTaO_2N$	Reported	0	1.83	0.55	−0.05
$LaTiO_2N$	Reported	3	2.41	0.09	−1.09
$BaNbO_2N$	Reported	0	2.03	0.59	−0.21
$Ba_3Ta_2O_5N_2$	New	33	2.34	−0.64	−1.75
Ba_2TaO_3N	New	13	2.81	−0.37	−1.95
Sr_2NbO_3N	New	0	3.15	−0.33	−2.25
$Li_{14}Cr_2ON_8$	New	0	2.43	−0.18	−1.38
$Sr_2Ti_6O_{11}N_2$	New	36	2.86	−0.15	−1.78
$Ba_2Ti_6O_{11}N_2$	New	21	2.77	−0.11	−1.65
$La_2TiO_2N_2$	New	3	2.46	0.02	−1.21
Na_5MoO_4N	New	0	3.19	0.43	−1.53
$Na_4WO_2N_2$	New	0	2.95	0.78	−0.94
Li_5MoO_4N	New	24	2.61	1.08	−0.30
$Ca_5WO_2N_4$	New	0	3.26	1.71	−0.32

[a] The numbers in the column of "CB *vs.* H_2/H_2O" and "VB *vs.* O_2/H_2O" have the same meaning as in Table 1.

voltage. This result may explain the experimental observation that only H_2 evolution reaction is photo-catalyzed by $CaTaO_2N$, $SrTaO_2N$, and $BaTaO_2N$ in ref. 49.

The remaining eleven materials, $Ba_3Ta_2O_5N_2$, Ba_2TaO_3N, Sr_2NbO_3N, $Li_{14}Cr_2ON_8$, $Sr_2Ti_6O_{11}N_2$, $Ba_2Ti_6O_{11}N_2$, $La_2TiO_2N_2$, Na_5MoO_4N, $Na_4WO_2N_2$, Li_5MoO_4N, and $Ca_5WO_2N_4$, have not been reported as water-splitting photocatalysts yet. $Li_{14}Cr_2ON_8$, Na_5MoO_4N, $Na_4WO_2N_2$, and $Ca_5WO_2N_4$ can be found in the ICSD with a known crystal structure. Ba_2TaO_3N and Sr_2NbO_3N are not in the ICSD but have been synthesized in ref. 53. Both their structures are declared as a K_2NiF_4 structure. This agrees with our computation as we derived both materials from a Sr_2SnO_4 structure prototype, which is closely related to K_2NiF_4. The other five candidates, $Ba_3Ta_2O_5N_2$, $Sr_2Ti_6O_{11}N_2$, $Ba_2Ti_6O_{11}N_2$, $La_2TiO_2N_2$, and Li_5MoO_4N, are predicted by us. $Ba_3Ta_2O_5N_2$ is derived from $Sr_3Ti_2O_7$. $Sr_2Ti_6O_{11}N_2$ and $Ba_2Ti_6O_{11}N_2$ are derived from $K_2Ti_6O_{13}$. $La_2TiO_2N_2$ is derived from Sr_2SnO_4. Li_5MoO_4N comes from a substitution of Na with Li in Na_5MoO_4N. We compared their crystal structures in Fig. 9–12 respectively. The instability energy ΔH for $Ba_3Ta_2O_5N_2$, $Sr_2Ti_6O_{11}N_2$, $Ba_2Ti_6O_{11}N_2$, $La_2TiO_2N_2$, and Li_5MoO_4N is 33 meV per atom, 35 meV per atom, 21 meV per atom, 3 meV per atom and 24 meV per atom respectively.

The band edge positions of these eleven interesting quaternary compounds are shown in Fig. 13, which suggests that, among them, $La_2TiO_2N_2$ and Li_5MoO_4N have the best band properties for a visible light driven photocatalyst. For both, the CB and VB are bracketing the water redox levels, and their band gap is predicted to be 2.46 eV and 2.61 eV respectively. The CB and VB of $Na_4WO_2N_2$ and $Ca_5WO_2N_4$ also bracket the water redox level, but their band gaps are too large for visible light absorption. However, similar to $Zr_3O_3N_2$, their large band gaps are mainly due to a too high CB level. Hence, if their CB levels can be shifted downwards by cation doping or solid solution, they may still become promising for visible-light driven photocatalysis. In contrast, $Ba_3Ta_2O_5N_2$ and $Li_{14}Cr_2ON_8$ have small enough band gaps for visible light absorption, but their CB levels are lower than the H_2/H_2O level, indicating that either an external bias voltage or CB engineering is needed to achieve water-splitting. It is worth noting that the CB level of $Li_{14}Cr_2ON_8$ is only 0.18 V lower than the H_2/H_2O level, indicating that the bias voltage required is small. The remaining five materials, Ba_2TaO_3N, Sr_2NbO_3N, $Sr_2Ti_6O_{11}N_2$, $Ba_2Ti_6O_{11}N_2$, and
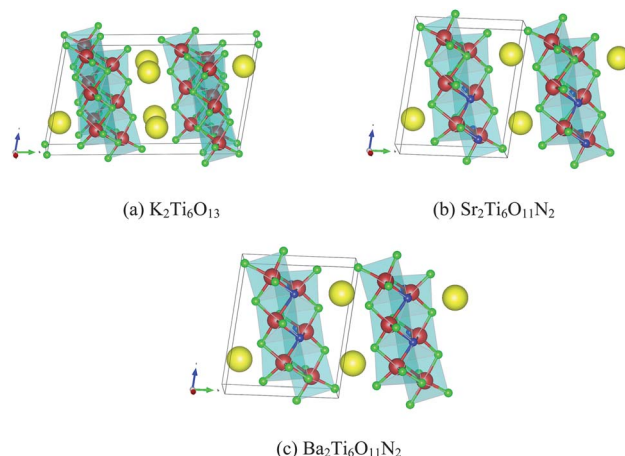
Fig. 10 Crystal structures of (a) $K_2Ti_6O_{13}$, (b) $Sr_2Ti_6O_{11}N_2$, and (c) $Ba_2Ti_6O_{11}N_2$. Blue atoms are N, green atoms are O, red atoms are Ti, and yellow atoms are (a) K, (b) Sr, and (c) Ba. Structures (b) and (c) are generated by substitution of all K atoms in (a) with Sr atoms and Ba atoms respectively, and 2/13 of the O atoms in (a) with N atoms.
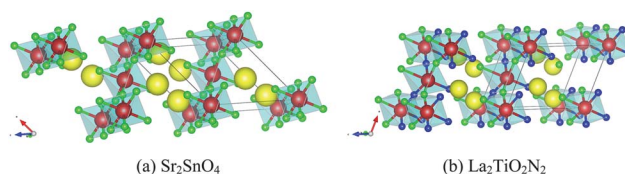

Fig. 11 Crystal structures of (a) Sr_2SnO_4 and (b) $La_2TiO_2N_2$. Blue atoms are N, green atoms are O, red atoms are (a) Sn and (b) Ti, and yellow atoms are (a) Sr and (b) La. Structure (b) is generated by substitution of all Sr atoms in (a) with La atoms, all Sn atoms in (a) with Ti atoms, and 1/2 of the O atoms in (a) with N atoms.
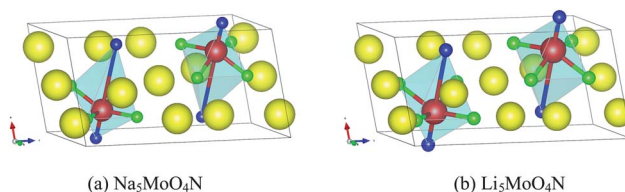

Fig. 12 Crystal structures of (a) Na_5MoO_4N and (b) Li_5MoO_4N. Blue atoms are N, green atoms are O, red atoms are Mo, and yellow atoms are (a) Na and (b) Li. Structure (b) is generated by substitution of all Na atoms in (a) with Li atoms.
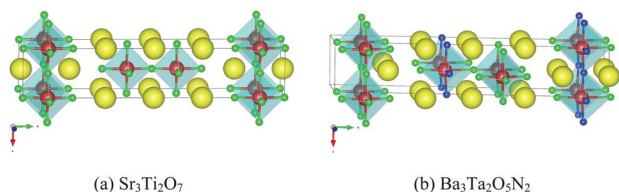
Na_5MoO_4N, are promising candidates for photocatalysts under UV illumination.

In this section, we identified seventeen materials, listed in Table 3, as promising candidates for photocatalysts. $CaTaO_2N$, $SrTaO_2N$, $BaTaO_2N$, $LaTaO_2N$, $LaTiO_2N$, and $BaNaO_2N$ have been reported as water splitting photocatalysts while the other eleven materials, $Ba_3Ta_2O_5N_2$, Ba_2TaO_3N, Sr_2NbO_3N, $Li_{14}Cr_2ON_8$, $Sr_2Ti_6O_{11}N_2$, $Ba_2Ti_6O_{11}N_2$, $La_2TiO_2N_2$, Na_5MoO_4N, $Na_4WO_2N_2$, Li_5MoO_4N, and $Ca_5WO_2N_4$, are newly identified in this paper. Among these eleven materials, $La_2TiO_2N_2$ and Li_5MoO_4N have the most promising band gap and band edge positions. Similar to $Ti_3O_3N_2$, they have the potential to be

Fig. 9 Crystal structures of (a) $Sr_3Ti_2O_7$ and (b) $Ba_3Ta_2O_5N_2$. Blue atoms are N, green atoms are O, red atoms are (a) Ti and (b) Ta, and yellow atoms are (a) Sr and (b) Ba. Structure (b) is generated by substitution of all Sr atoms in (a) with Ba atoms, all Ti atoms in (a) with Ta atoms, and 2/7 of the O atoms in (a) with N atoms.

164 | *Energy Environ. Sci.*, 2013, **6**, 157–168

This journal is © The Royal Society of Chemistry 2013

Fig. 13 Band edge positions of $Ba_3Ta_2O_5N_2$, Ba_2TaO_3N, Sr_2NbO_3N, $Li_{14}Cr_2ON_8$, $Sr_2Ti_6O_{11}N_2$, $Ba_2Ti_6O_{11}N_2$, $La_2TiO_2N_2$, Na_5MoO_4N, $Na_4WO_2N_2$, Li_5MoO_4N, and $Ca_5WO_2N_4$ in the normal hydrogen electrode (NHE) reference. The solid blue lines indicate the CB levels and the solid red lines indicate the VB levels.

better water splitting photocatalysts than TaON. $Na_4WO_2N_2$ and $Ca_5WO_2N_4$ have a band gap too large for visible light absorption and can work under UV light illumination. However, with some CB engineering, they may still be promising visible light driven photocatalysts. $Ba_3Ta_2O_5N_2$ and $Li_{14}Cr_2ON_8$ have a good band gap for visible light absorption, but they need an external bias voltage to photo-catalyze the H_2 evolution reaction. In addition, Ba_2TaO_3N, Sr_2NbO_3N and $La_2TiO_2N_2$ have the same crystal structure (Sr_2SnO_4 structure). Therefore, the solid solutions of these three materials are also likely to be synthesizable and are likely to be promising candidates for water-splitting photocatalysts as well.

IV Discussion

We demonstrated in this paper a high throughput computational screening for the design of novel water-splitting photocatalysts. Compounds are screened based on their phase stability, band gap, and band edge positions in aqueous environment. Eleven known photocatalysts are reproduced and sixteen new candidate photocatalysts are proposed by our screening, indicating the validity of the approach. However, it is worth noting that there are other important properties not considered in our screening. The aqueous stability of a material is important for the commercial exploitation of a photocatalyst. The standard tool to estimate it is the Pourbaix diagram.[54] However, Pourbaix diagrams have only been determined for elements in equilibrium with water. To assess the stability of more complex materials in water, one could use a recently developed method which enables the construction of Pourbaix diagrams almost entirely from first principles.[55] The method

treats the Pourbaix diagram as a phase stability diagram for a material in equilibrium with various aqueous species.

Our screening does not consider kinetic properties either, but they also affect the performance of photocatalysts. For instance, one major issue for hematite Fe_2O_3, a promising visible light driven photocatalyst, is its poor charge carrier diffusion.[56] Defect related properties are also not considered in this paper. Defect formation energy and defect concentration are closely related to the charge carrier recombination rate and lifetime, thus having an effect on the efficiency of the device. Dopability suggests to which extent the material can be engineered for a given dopant and also indicates how strong the innate P–N junction field could be designed to help the electron–hole separation. For these properties, the *ab initio* predictions are often too expensive to be included in a high throughput screening system, but they could be investigated specifically for the new candidates. Another limitation is that, in this paper, the properties are predicted under dark conditions. However, a photocatalyst works in an illuminated environment, and thus some of its properties such as band edge positions may change accordingly.

As we mentioned in Section III.2, Fig. 5 suggests that V^{5+}, Cr^{6+}, Mo^{6+}, and Sb^{5+} do not form any stable ternary oxynitrides. We believe that this is because the required oxidizing power for these cations is too large to achieve with nitrogen. Fig. 14 illustrates this. For each cation in Fig. 14, we analyzed the thermodynamic phase stability of the binary oxide with the cation under different oxygen chemical potentials and thus evaluated the minimum oxygen chemical potential required to form a stable binary oxide with the cation. A higher minimum chemical potential indicates a larger oxidizing power required for the cation. While equivalent data for nitrides are not available, the oxide data in Fig. 14 should be representative of the relative oxidation strength needed. Fig. 14 shows that V^{5+}, Cr^{6+}, Mo^{6+}, and Sb^{5+} require the largest oxidizing power among these cations. Moreover, these four cations do not have corresponding binary nitrides in the ICSD, supporting the observation we made in Fig. 5. It is worth noting that we found stable quaternary oxynitrides with Cr^{6+}, Mo^{6+}, and Sb^{5+} in Fig. 8, indicating that adding a second cation may reduce the oxidation power required.

The reason to use nitrogen instead of oxygen as the anion was to increase the valence band energy and lower the band gap.
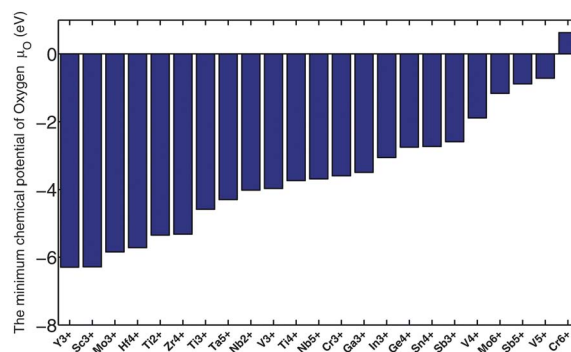

Fig. 14 Estimate of the oxidizing power required to create certain cations.

This journal is © The Royal Society of Chemistry 2013

Energy Environ. Sci., 2013, **6**, 157–168 | **165**

It is therefore interesting to investigate the extent of the band gap reduction as one goes from oxide to oxynitride. To study this question, we take the lowest energy structure for each ternary oxynitride that we generated in Section III.2, and compare its computed band gap to the experimentally measured gap of the binary oxide with the same cation. We collected the experimental gaps from ref. 3, 16 and 57–69. For example, for Ta^{5+}, we compared the band gap of TaON, Ta_3O_6N, $Ta_4O_7N_2$, Ta_4ON_6, and $Ta_8O_{11}N_6$ to the experimentally measured band gap of Ta_2O_5. The reasons for using experimentally measured gaps but not computed band gaps as the binary oxide references are that (1) binary oxides are generally well studied in experiment, and thus their measured gaps are accessible and reliable; (2) we used the GGA+U based Δ-sol method[32] for computing the band gaps, and the U value is typically different between oxynitrides and oxides, so even if we compare the computed gaps of oxynitrides to the computed gaps of binary oxides, the comparison would not be consistent as it is based on different U parameters. A histogram of the band gap reduction for all generated ternary oxynitride compounds is shown in Fig. 15. Note that we only generated ternary oxynitride containing d^0 or d^{10} cations. The mean band gap reduction is around 1.8 eV. This verifies that by introducing N into an oxide, the band gap can be significantly reduced. It is worth noting that the range of the band gap reduction is fairly large, from 0 eV to 4 eV. This large range could be due to two reasons. The first reason may be that the effect depends substantially on the cation. The second reason may be that, even for the same cation, introducing different amounts of nitrogen into the system may lead to different band gap reductions. To better demonstrate these two factors, we plot the band gap reduction for each cation in Fig. 16. We see clearly that the mean band gap reduction is generally different for different cations, and this difference is on the order of 1 eV. In the meantime, the standard deviation of the band gap reduction for a given cation is sometimes also on the order of 1 eV. This observation indicates that the two facts mentioned above both influence the band gap reduction.

We look further into the effect of the amount of nitrogen on the band gap reduction. It is possible that a change of the N/O ratio gives a different O_{2p} and N_{2p} weight in the valence band,
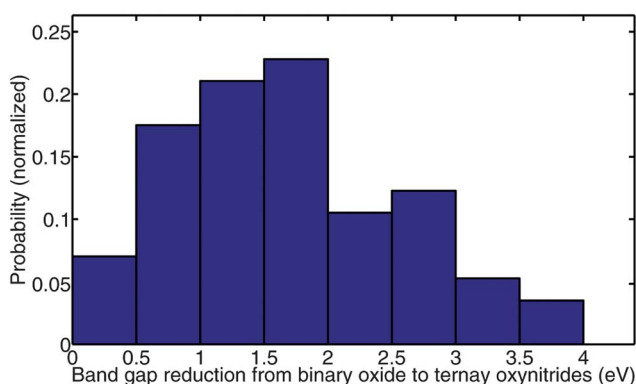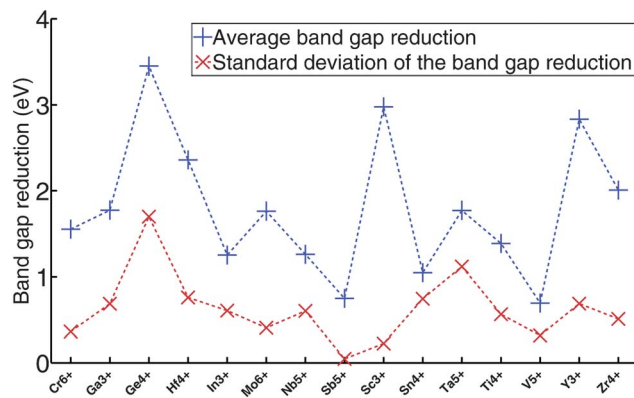

Fig. 16 The blue line is the band gap reduction for each cation. The red line is the standard deviation of the band gap reduction for each cation.
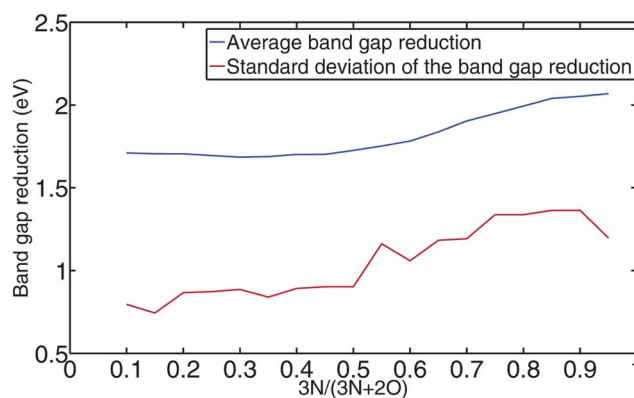

Fig. 17 The blue line is the average band gap reduction as a function of the N/O ratio. The red line is the standard deviation of the band gap reduction at a given N/O ratio.

thus leading to a different band gap reduction. Alternatively, a different amount of nitrogen may lead to different crystal structures and thus to a different band gap reduction. Fig. 17 shows the average band gap reduction and its standard deviation as a function of the N/O ratio. We observe that the average band gap reduction does not change much with the N/O ratio. From a very small ratio of N/O (left end of the blue line in Fig. 17) to a very large ratio of N/O (right end of the blue line in Fig. 17), the average band gap reduction changes about 0.4 eV. The rest of the difference in band gap reduction, which is on the order of 1 eV, comes from the crystal structure change. As an extension of this observation, we would like to point out that adding more nitrogen into an oxide system does not necessarily lead to a larger band gap reduction as one might assume, because this statement does not consider the effect of the possible crystal structure change. For instance, our computation suggests that the band gap of $Nb_4O_7N_2$ is less than that of Nb_4ON_6 (1.52 eV vs. 1.85 eV).

V   Conclusion

In this paper, we presented a high throughput first principle approach to search for new water-splitting photocatalysts, and

Fig. 15 A histogram of band gap reduction from d^0 and d^{10} binary oxides to ternay oxynitrides.

applied it to oxynitrides and some nitrides. Most of the known photocatalytic materials in the screened chemical space are reproduced, proving the validity of the approach. In addition, sixteen new materials are suggested as promising photocatalysts, including three binary nitrides, two ternary oxynitrides and eleven quaternary oxynitrides. They have been either synthesized experimentally or predicted, by our approach, to be synthesizable. Because of their predicted band gap and band edge positions, $Ti_3O_3N_2$, $La_2TiO_2N_2$ and Li_5MoO_4N are particularly promising as visible light driven photocatalysts. In addition, with some further CB engineering or a small bias voltage, Cu_3N, $Zr_3O_3N_2$, $Ba_3Ta_2O_5N_2$, $Li_{14}Cr_2ON_8$, $Na_4WO_2N_2$, and $Ca_5WO_2N_4$ also have the potential to be good visible light driven photocatalysts. The remaining seven materials, AgN_3, Zr_3N_4, Ba_2TaO_3N, Sr_2NbO_3N, $Sr_2Ti_6O_{11}N_2$, $Ba_2Ti_6O_{11}N_2$, and Na_5MoO_4N, are candidates for photocatalysts that may work under UV illumination. In addition, based on our screening result, the solid solutions of $Ti_3O_3N_2$, $Zr_3O_3N_2$, and Ta_3N_5 and the solid solutions of Ba_2TaO_3N, Sr_2NbO_3N and $La_2TiO_2N_2$ may be synthesizable and may be promising candidates for photocatalysts too.

Acknowledgements

References

1 A. Fujishima and K. Honda, *Nature*, 1972, **238**(5358), 37.

2 A. Fujishima and K. Honda, *Bull. Chem. Soc. Jpn.*, 1971, **44**(4), 1148.

3 F. E. Osterloh, *Chem. Mater.*, 2008, **20**, 35–54.

4 G. Hautier, A. Jain, S. P. Ong, B. Kang, C. Moore, R. Doe and G. Ceder, *Chem. Mater.*, 2011, **23**, 3495–3508.

5 A. Jain, G. Hautier, C. Moore, B. Kang, J. Lee, H. Chen, N. Twu and G. Ceder, *J. Electrochem. Soc.*, 2012, **159**(5), A622–A633.

6 H. Chen, G. Hautier, A. Jain, C. Moore, B. Kang, R. Doe, L. Wu, Y. Zhu, Y. Tang and G. Ceder, *Chem. Mater.*, 2012, **24**(11), 2009–2016.

7 G. Hautier, A. Jain, H. Chen, C. Moore, S. P. Ong and G. Ceder, *J. Mater. Chem.*, 2011, **21**, 17147–17153.

8 S. Wang, Z. Wang, W. Setyawan, N. Mingo and S. Curtarolo, *Phys. Rev. X*, 2011, **1**, 021012.

9 G. K. H. Madsen, *J. Am. Chem. Soc.*, 2006, **128**, 12140–12146.

10 R. Armiento, B. Kozinsky, M. Fornari and G. Ceder, *Phys. Rev. B: Condens. Matter Mater. Phys.*, 2011, **84**, 014103.

11 J. Hachmann, R. Olivares-Amaya, S. Atahan-Evrenk, C. Amador-Bedolla, R. S. Sanchez-Carrera, A. Gold-Parker, L. Vogt, A. M. Brockway and A. Aspuru-Guzik, *J. Phys. Chem. Lett.*, 2011, **2**, 2241–2251.

12 A. N. Sokolov, S. Atahan-Evrenk, R. Mondal1, H. B. Akkerman, R. S. Sánchez-Carrera, S. Granados-Focil, J. Schrier, S. C. B. Mannsfeld, A. P. Zoombelt, Z. Bao and A. Aspuru-Guzik, *Nat. Commun.*, 2011, **2**, 432.

13 N. M. O'Boyle, C. M. Campbell and G. R. Hutchison, *J. Phys. Chem. C*, 2011, **115**, 16200–16210.

14 A. Jain, G. Hautier, C. J. Moore, S. P. Ong, C. C. Fischer, T. Mueller, K. A. Persson and G. Ceder, *Comput. Mater. Sci.*, 2011, **50**, 2295–2310.

15 G. Ceder, G. Hautier, A. Jain and S. P. Ong, *MRS Bull.*, 2011, **36**(3), 185–191.

16 K. Maeda and K. Domen, *J. Phys. Chem. C*, 2007, **111**, 22.

17 D. Yokoyama, H. Hashiguchi, K. Maeda, T. Minegishi, T. Takata, R. Abe, J. Kubota and K. Domen, *Thin Solid Films*, 2011, **519**, 2087–2092.

18 Inorganic Crystal Structure Database, http://icsd.fiz-karlsruhe.de/icsd/.

19 G. Hautier, C. Fischer, V. Ehrlacher, A. Jain and G. Ceder, *Inorg. Chem.*, 2011, **50**, 656–663.

20 I. E. Castelli, T. Olsen, S. Datta, D. D. Landis, S. Dahl, K. S. Thygesena and K. W. Jacobsen, *Energy Environ. Sci.*, 2012, **5**, 5814.

21 P. Hohenberg and W. Kohn, *Phys. Rev.*, 1964, **136**(21), B864.

22 W. Kohn and L. J. Sham, *Phys. Rev.*, 1965, **140**, A1133.

23 P. E. Blöchl, *Phys. Rev. B: Condens. Matter Mater. Phys.*, 1994, **50**, 17953–17979.

24 G. Kresse and J. Furthmuller, *Phys. Rev. B: Condens. Matter Mater. Phys.*, 1996, **54**(11), 169.

25 G. Kresse and D. Joubert, *Phys. Rev.*, 1999, **59**, 1758.

26 J. P. Perdew, K. Burke and M. Ernzerhof, *Phys. Rev. Lett.*, 1996, **77**, 3865.

27 Y. Wu, M. K. Y. Chan and G. Ceder, *Phys. Rev. B: Condens. Matter Mater. Phys.*, 2011, **83**, 235301.

28 G. L. W. Hart and R. W. Forcade, *Phys. Rev. B: Condens. Matter Mater. Phys.*, 2008, **77**(22), 1–12.

29 M. Yang, J. Oró-Solé, J. A. Rodgers, A. B. Jorge, A. Fuertes and J. P. Attfield, *Nat. Chem.*, 2011, **3**(1), 47–52.

30 G. Hautier, S. P. Ong, A. Jain, C. J. Moore and G. Ceder, *Phys. Rev. B: Condens. Matter Mater. Phys.*, 2012, **85**, 155208.

31 A. Jain, G. Hautier, S. P. Ong, C. J. Moore, C. C. Fischer, K. A. Persson and G. Ceder, *Phys. Rev. B: Condens. Matter Mater. Phys.*, 2011, **84**, 045115.

32 M. K. Y. Chan and G. Ceder, *Phys. Rev. Lett.*, 2010, **105**, 196403.

33 M. S. Wrighton, D. S. Ginley, P. T. Wolczanski, A. B. Ellis, D. L. Morse and A. Linz, *Proc. Natl. Acad. Sci. U. S. A.*, 1976, **72**(4), 1518.

34 M. G. Walter, E. L. Warren, J. R. McKone, S. W. Boettcher, Q. Mi, E. A. Santori and N. S. Lewis, *Chem. Rev.*, 2010, **110**, 6446–6473.

35 T. Lindgren, M. Larsson, S. E. Lindquist, *Proc. 14th Int. Workshop on Quantum Solar Energy Conversion*, 2002.

36 H. A. Al-Brithen, A. R. Smith and D. Gall, *J. Appl. Phys.*, 2001, **90**, 4.

37 L. Bergman, X. B. Chen, D. McIlroy and R. F. Davis, *Appl. Phys. Lett.*, 2002, **81**, 22.

This journal is © The Royal Society of Chemistry 2013

Energy Environ. Sci., 2013, **6**, 157–168 | **167**

38 M. Hara, G. Hitoki, T. Takata, J. N. Kondo, H. Kobayashi and K. Domen, *Catal. Today*, 2003, **78**, 555–560.

39 M. Bär, K. S. Ahn, S. Shet, Y. Yan, L. Weinhardt, O. Fuchs, M. Blum, S. Pookpanratana, K. George, W. Yang, J. D. Denlinger, M. Al-Jassim and C. Heske, *Appl. Phys. Lett.*, 2009, **94**, 012110.

40 J. S. Becker, E. Kim and R. G. Gordon, *Chem. Mater.*, 2004, **16**, 3497–3501.

41 C. S. Rees and M. M. Chaudhri, *J. Phys. C: Solid State Phys.*, 1987, **20**, 4097–4104.

42 P. Kroll, *Phys. Rev. Lett.*, 2003, **90**(12), 125501.

43 J. J. Chen, B. P. Gila, M. Hlad, A. Gerger, F. Ren, C. R. Abernathy and S. J. Peartona, *Appl. Phys. Lett.*, 2006, **88**, 042113.

44 K. Maeda, T. Takata, M. Hara, N. Saito, Y. Inoue, H. Kobayashi and K. Domen, *J. Am. Chem. Soc.*, 2005, **127**, 8286–8287.

45 J. Sato, N. Saito, Y. Yamada, K. Maeda, T. Takata, J. N. Kondo, M. Hara, H. Kobayashi, K. Domen and Y. Inoue, *J. Am. Chem. Soc.*, 2005, **127**, 4150–4151.

46 T. Mishima, M. Matsuda and M. Miyake, *Appl. Catal., A*, 2007, **324**, 77–82.

47 http://www.titandioxide.ru/titan_s/sc3/0176.php.

48 K. Maeda, M. Higashi, B. Siritanaratkul, R. Abe and K. Domen, *J. Am. Chem. Soc.*, 2011, **133**, 12334–12337.

49 D. Yamasita, T. Takata, M. Hara, J. N. Kondo and K. Domen, *Solid State Ionics*, 2004, **172**, 591.

50 G. Hitoki, T. Takata, J. N. Kondo, M. Hara, H. Kobayashi and K. Domen, *Electrochemistry*, 2002, **70**, 463.

51 A. Kasahara, K. Nukumizu, G. Hitoki, T. Takata, J. N. Kondo, M. Hara, H. Kobayashi and K. Domen, *J. Phys. Chem. A*, 2002, **106**, 6750.

52 B. Siritanaratkul, K. Maeda, T. Hisatomi and K. Domen, *ChemSusChem*, 2011, **4**, 74–78.

53 G. Tobías, D. Beltrán-Porter, O. I. Lebedev, G. Van Tendeloo, J. Rodríguez-Carvajal and A. Fuertes, *Inorg. Chem.*, 2004, **43**(25), 8011.

54 M. Pourbaix, *Atlas of Electrochemical Equilibria in Aqueous Solutions*, National Association of Corrosion Engineers, Houston, Texas, 1974.

55 K. A. Persson, B. Waldwick, P. Lazic and G. Ceder, *Phys. Rev. B: Condens. Matter Mater. Phys.*, 2012, **85**, 235438.

56 M. P. Dare-Edwards, J. P. Goodnough, A. Hamnett and P. R. Trevellick, *J. Chem. Soc., Faraday Trans.*, 1983, **79**, 2027–2041.

57 H. J. Zhai, S. Li, D. A. Dixon and L. S. Wang, *J. Am. Chem. Soc.*, 2008, **9**(130), 15.

58 M. Higashiwaki, K. Sasaki, A. Kuramata, T. Masui and S. Yamakoshi, *Appl. Phys. Lett.*, 2012, **100**, 013504.

59 A. S. Zyubin, A. M. Mebel and S. H. Lin, *J. Phys. Chem. A*, 2007, **111**, 38.

60 W. J. Zhu, T. Tamagawa, M. Gibson, T. Furukawa and T. P. Ma, *IEEE Electron Device Lett.*, 2002, **23**, 11.

61 L. F. J. Piper, A. DeMasi, S. W. Cho, K. E. Smith, F. Fuchs, F. Bechstedt, C. Körber, A. Klein, D. J. Payne and R. G. Egdell, *Appl. Phys. Lett.*, 2009, **94**, 022105.

62 L. Mai, B. Hu, W. Chen, Y. Qi, C. Lao, R. Yang, Y. Dai and Z. L. Wang, *Adv. Mater.*, 2007, **19**, 3712–3716.

63 E. Z. Kurmaev, A. Moewes, O. G. Bureev, I. A. Nekrasov, V. M. Cherkashenko, M. A. Korotin and D. L. Ederer, *J. Alloys Compd.*, 2002, **347**, 213–218.

64 A. Nainani, Y. Sun, T. Irisawa, Z. Yuan, M. Kobayashi, P. Pianetta, B. R. Bennett, J. B. Boos and K. C. Saraswat, *J. Appl. Phys.*, 2011, **109**, 114908.

65 A. V. Emeline, E. V. Lobyntseva, V. K. Ryabchuk and N. Serpone, *J. Phys. Chem. B*, 1999, **103**, 1325–1331.

66 Ç. Kılıç and A. Zunger, *Phys. Rev. Lett.*, 2002, **88**, 095501.

67 A. Chakrabarti, K. Hermann, R. Druzinic, M. Witko, F. Wagner and M. Petersen, *Phys. Rev. B: Condens. Matter Mater. Phys.*, 1999, **59**, 16.

68 D. Jia., X. Wang and W. M. Yen, *Phys. Rev. B: Condens. Matter Mater. Phys.*, 2004, **69**, 235113.

69 A. Emeline, G. V. Kataeva, A. S. Litke, A. V. Rudakova, V. K. Ryabchuk and N. Serpone, *Langmuir*, 1998, **14**, 5011–5022.

168 | *Energy Environ. Sci.*, 2013, **6**, 157–168

This journal is © The Royal Society of Chemistry 2013